Chapter 2

Rigidity and flexibility of glassy networks and fast-ion conduction

M. Malki[a,b], M. Micoulaut[c], Deassy Novita[d], B.Goodman[e], P. Boolchand[d,e]

[a]*CEMHTI, UPR CNRS 3079, 1D Avenue de la Recherche Scientifique, 45071 Orléans Cedex 02, France*
[b]*Polytech' Orléans, 8, rue Léonard de Vinci, 45072 Orléans Cedex 05 France*
[c]*Laboratoire de Physique Théorique de la Matière Condensée, UPMC-Paris 6, 4, Place Jussieu, 75252 Paris Cedex 05 France*
[d]*Department of Electrical and Computer Engineering and Computer Science, University of Cincinnati, Cincinnati, OH 45221-0030, USA*
[e]*Department of Physics, University of Cincinnati, Cincinnati, OH 45221- 0011, USA*

The ionic conductivity (σ_{ionic}) of amorphous electrolytes (glasses) is related here to the mechanical nature of the host network and, accordingly, displays three distinct elastic regimes common to glass networks, namely, a flexible, an intermediate and a stressed-rigid phase. It is shown that the onset of conduction at higher modifying-ion content results from the breakdown of rigidity as well as from the increase in free-carrier density. A derivation of σ_{ionic} is presented here, which incorporates network rigidity explicitly; and the results are compared quantitatively with experimental data.

1. Introduction

Gaining a better understanding of electrical transport in fast ionic conductors such as amorphous electrolytes is a basic scientific challenge, with potential important technological applications. Oxide or chalcogenide based amorphous materials can display high electrical conductivities, and the

Series: Optoelectronic Materials and Devices, ISSN 1584-5508
Volume 6, 2009, Rigidity and Boolchand intermediate phases in nanomaterials, ISBN 13/978-973-88109-4-5

materials have found application in solid state batteries, sensors, and non-volatile memory devices [1]. In order to tune their physical properties for applications, one has to better understand how chemistry *via* molecular structure, controls conductivity and the underlying conduction mechanisms.

The conductivity can be expressed in terms of the free carrier density n_L and the carrier mobility □□ by: □= Ze □□n with *Ze* the charge of the conducting ion. It seems that theoretical approaches to ionic conduction in glasses have concentrated either on the dominant role of the free carrier density n_L [2] or of the carrier mobility [3, 4]. The added ionic species are network modifiers and can substantially change the mechanical nature of the host network. Therefore, the two effects must be considered together.

It is generally believed [5-8] that, in solid electrolyte *glasses*, physical processes associated with ion transport and with network structure are *decoupled*. This view is based on the enormously disparate time scales involved in charge relaxation vs structural rearrangement relaxation. For example, the ratio (R_τ) of structural ($\tau_s \sim 10^2$ sec) to conductivity ($\tau_\sigma \sim 10^{-10}$ sec) relaxation times near the glass transition temperature (T_g) is of the order of $R_\tau \sim 10^{12}$. On the other hand, in polymer electrolytes such as polyalkylene oxides, R_τ values of nearly 1 or even less than 1 have been observed [8, 9]. In these *coupled* systems, according to [5-8], clearly a reverse circumstance must prevail, viz., ion-hopping and network structure relaxation must be closely tied to each other.

However, recently Ingram et al. [10] have argued that the dichotomy between *coupled* charge transport vs structural relaxation behavior and apparently *decoupled* behavior is *not* fundamental. In fact they are not even very different quantitatively when the measured quantities are expressed in terms of activation energies E_A (A= s, σ) and activation volumes V_A. Experimentally, Ingram et al present new data from conductivity and pressure-DSC experiments on the *decoupled* glassy electrolyte system, $(AgI)_{50}(Ag_2O)_{25}(MoO_3)_{25}$ (Ag-iodomolybdate),. By an analysis, which we will not go into here, they are able to extract the four activation numbers, E(s,σ) and V(s,σ). They also present the corresponding values for some *coupled* polymeric electrolytes and show that the activation ratios just near T_g,, namely,

$$M_A = E_A / V_A \qquad (1)$$

are of the same order for *all* the systems considered. For the polymers, M^P_σ and M^P_s were esentially independent of temperature so that the E vs V plots are linear. For the glasses, the values of M^G_σ and M^G_s both lie between 7 to 8 MPa. For each of the polymers, M^P_σ and M^P_s are also nearly equal and, though the M^P values differ from polymer to polymer, they are all of the same order as M^G; despite their 'bare' R_τ values being many orders of

magnitude smaller – of order unity – than of order 10^{12} for the glass. These disparate ratios are due to the fact that the τ_A's are exponential functions of E_A and V_A.

Ingram et al. [10] call M a *local modulus*, a generic and not atomically specific measure of the stresses involved in s and σ dynamical processes. For Ag-iodomolybdate M is about one third of the bulk modulus, which is consistent with the picture that a smaller number of nearby atoms is needed in response to a local change than for a distortion which extends throughout the bulk. (It may be sometimes conceptually helpful to think of M as a *local stress*, which it is dimensionally.)

Additional support for the view proposed in [10] derives from the relative magnitutes of estimated atomic displacements *l* involved in s and σ processes: If we put $V \sim l^3$, then the ratio V_s/V_σ, which is roughly 64 in Ag-iodomolybdate, means that l^G_σ = ¼ l^G_s - which is not unreasonable. Furthermore, their Table 1 gives the value V_s = 174 cm^3/mol, and this translates via Avogrado's number to 0.29 nm^3/ molecule, or l^G_s = 0.66nm (6.6A) and l^G_σ = 0.16nm (1.6A), both of which are also plausible values.

With ionic conduction dependent on the mechanical nature of the glass network, we should expect it to show the now generally recognized elastic phases: flexible, IP and stressed rigid. Threshold behaviour was seen earlier in fast ionic conductors, but the connection with rigidity transitions was not recognized. The boundaries of the IP, expressed in terms of network mean coordination numbers $\bar{r}_{c(1)}$ and $\bar{r}_{c(2)}$ have been characterized from experiments for many different systems [11-16], numerical calculations [17, 18], cluster analysis [19, 20] and energy adaptation [21] and identified as being a rigidity transition at $\bar{r}_{c(1)}$ and a stress transition at $\bar{r}_{c(2)} > \bar{r}_{c(1)}$. In random networks both transitions coalesce into a single threshold near $\bar{r} = 2.4$. Maxwell constraint counting [22] predicts the vanishing of the number of floppy modes [23, 24], i.e. the low energy modes that serve to locally deform the network vanish at the single threshold. Up to now, signatures of the two transitions have been detected in calorimetric [11-15] and in vibrational spectroscopic probes [16].

In the remainder of this chapter a theory of ionic conductivity is presented in Section 2 which is based explicitly on features of the different elastic phases. The calculations are in reasonable accord with experimental results given in Section 3.

2. A rigidity based theory for ionic conduction

A model of ionic conduction is combined with the size increasing cluster model approach (SICA) to rigidity transitions, and as in ref.[19], this

allows us to study in detail the effect of elastic phases on ion conduction.A model of ionic conduction is combined with the size increasing cluster model approach (SICA) to rigidity transitions, and as in ref.[19], this allows us to study in detail the effect of the phase structure.

In stressed rigid electrolytes, the combination of a weak number of free carriers and a large strain energy for migration leads to very low conductivities whose order of magnitude is given by the Coulombic interaction between the carrier and its anionic site. Conductivity builds up in the IP where additional hopping processes appear. These new hopping processes are found on flexible parts (ion rich) of the network and do not exist in the stressed rigid phase. Finally, the lowering of the strain energy due to the presence of floppy modes that allow the local deformation of the network, promotes ease of conduction in the flexible phase.

2.1 Construction

Agglomeration of select local structures (tetrahedral, pyramids, atom pairs, etc) to produce larger molecular clusters (rings, edge-sharing tetrahedral units, chains, etc) emulating medium range order characteristic of real network glasses has proved to be a useful approach to understanding their flexibility and rigidity behavior. The size increasing cluster approximation (SICA), has for example, been useful in elucidating what aspects of local structures, such as corner-sharing and edge sharing

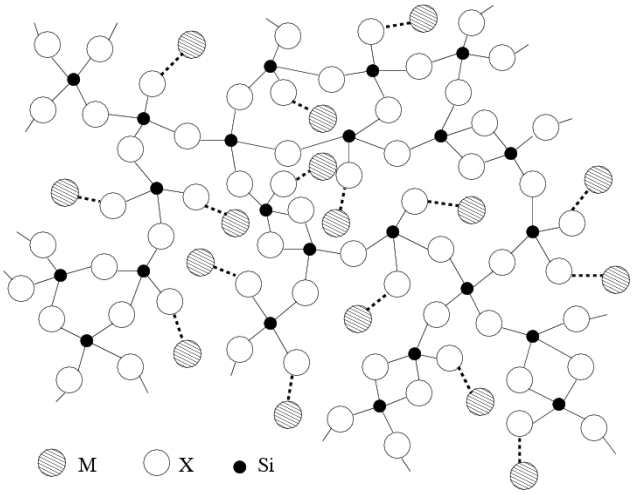

Fig. 1. A typical network of the form $(1-x)SiX_2$-xM_2X showing covalent Si-X and ionic M-X bonds. Here M = alkali atom, and X = O,S or Se. Note that this network contains edge-sharing tetrahedra that contribute to the width of the intermediate phase.

tetrahedral units, could be relevant in contributing to the onset of rigidity and stress phase transitions observed in binary Ge_xSe_{1-x} glasses. Here we use SICA [19, 20] to compute the probability of clusters in the three phases for glasses of the form $(1-x)SiX_2$-xM_2X with ($X=O,S,Se$ and $M=Li,Na,K,...$) which display a mean-field rigidity transition at $x=x_c=0.20$ [25]. These glasses serve as basic system for a number of fast ionic conductors (Fig. 1) and have a rather well-defined short-range order extracted from NMR experiments. The network consists indeed of $SiX_{4/2}$ and $SiX_{5/2}M$ tetrahedra (respectively termed as Q^4 and Q^3 in NMR notation [26, 27]) in the present concentration range of interest [$x=0$, $x=0.33$].

Using SICA, a network of N tetrahedra Q^4 and Q^3 with respective probabilities $(1-p)$ and $p=2x/(1-x)$ is considered at a basic step $l=1$. Note that a Q^4 unit is stressed rigid ($n_c=3.67$ per atom) whereas Q^3 is flexible ($n_c=2.56$ per atom). Starting from this short range order (the SICA building blocks), one can construct all possible structural arrangements to obtain clusters containing two Q^i's (step $l=2$), three Q^i's ($l=3$), etc. The various possible connections (Q^4-Q^4, Q^4-Q^3, Q^3-Q^3) define energy gains accordingly to their mechanical nature and their probabilities can be computed. Details of the method and application can be found elsewhere in this book. This allows to compute the floppy mode density $f^{(l)}$ of the network which, in the case of doublet pairs Q^j-Q^k (i.e. $l=2$) with probability p_{jk} , is given by:

$$f^{(2)} = 3 - n_c^{(2)} = 3 - \frac{\sum_{j,k} n_{c(jk)} p_{jk}}{\sum_{j,k} N_{jk} p_{jk}} \qquad (2)$$

where $n_{c(jk)}$ and N_{jk} are respectively the number of constraints and the number of atoms of a Q^j-Q^k pair. An intermediate phase is obtained if self-organization is achieved, i.e. if with growing connectivity all pairs with stress outside of cyclic (ring) structures can be avoided. In the present system, the only stressed rigid pair is the corner-sharing Q^4-Q^4 one (Fig. 2). In practice, one starts from a flexible network which is found at high modifier concentration x. If one decreases the modifier content, one will obtain more and more Q^4 species with still $f^{(2)}>0$. At a certain point in composition $x=x_r$, there will be enough of these structural units to ensure rigidity and allow $f^{(2)}$ to vanish. Stress is then only possible on Q^4-Q^4 pairs that form rings, i.e. edge-sharing structures which are weakly stressed rigid ($n_c=3.25$ per atom) and isostatically rigid ($n_c=3.0$ per atom) in the case of an infinite edge-sharing tetrahedral chain. With this selection rule in the cluster construction, one can still reduce the concentration x beyond the rigidity transition and obtain a network that is almost stress-free. But the selection rule holds only down to a certain point in composition $x=x_s$ below which

corner-sharing Q^4-Q^4 pairs cannot be avoided anymore. Stress is then able to percolate across the network. The IP is defined between a lower modifier concentration x_s and an upper value x_r ;and its width is given by $\Delta x = x_r - x_s$. In this approach, the width is found to depend mostly on the fraction of ES tetrahedra. Results of such an application to the present system are given elsewhere

Our theory of ionic conduction builds on the Anderson-Stuart model [28] which separates the activation energy for ionic conduction into an electrostatic and migration part E_c and E_m that respectively contribute to the free carrier density n_L and the carrier mobility □, respectively. In this mod
the low temperature Arrhenius behaviour of the conductivity [29, 30] is written as:

$$\sigma(T) = \frac{\sigma_0}{T} e^{-E_A / k_B T} = \frac{\sigma_0}{T} e^{-(E_C + E_m)/k_B T} \tag{3}$$

In the following, we concentrate our efforts on the energies E_c and E_m which can be directly related to the statistics of clusters and the enumeration of constraints. Next, one evaluates the free carrier rate n_L. On each Q^j-Q^k pair, there is a probability to find *n=0, 1 or 2* vacancies (see Fig. 2) which will contribute to the free carrier concentration. A mean Coulombic energy can be computed over all possible pairs with probability p_{jk}, that lead to the free carrier rate:

$$n_L^{(2)} = 2xe^{-\beta < E_c >} \tag{4}$$

with:

$$< E_c > = \frac{1}{Z} \sum_{j,k} \sum_{n} n E_c \, p_{jk} e^{-\beta n E_c} \tag{5}$$

where E_c is the Coulombic energy to extract the cation *M* from the anionic site *X* (*X=0,S,Se*) and acts as a free parameter for the theory [31]. *Z* normalizes the free carrier concentration in order to have $n_L^{(2)}=0$ at *T=0* and $n_L^{(2)}=2x$, the maximum possible carrier concentration, at infinite temperature As the probability p_{jk} of pairs will depend on the nature of the elastic phase, should depend also be different in the three phases (flexible, intermediate, stressed). In the concentration range of interest, one possible environment for the M^+ carriers is identified, the Q^3 unit corresponding to singly occupied negative sites (e.g. a non-bridging oxygen, NBO) whose number changes with *x* according to the structural change of the network [32].

Once a carrier is free to move, it is supposed to hop between two vacant sites and the general form for hopping rates is usually given by

$J_{ij}=\nu_{ij}\exp[-E_m/k_BT]$ with ν_{ij} an attempt frequency [33] depending on the local environment of the hopping cation which is constant here as only one type of Q^n species ($n=3$) is involved in the ionic conduction. The strain or migration energy E_m for the hop is roughly the energy required to locally deform the network between the cation and a vacant site [34]. It should therefore depend on the floppy mode energy and does not depend on the process (i,j). This amounts to neglect of the Coulombic repulsion from vacant sites. Note that, for the stressed rigid phase, there are only few hopping sites involved as the network is made only of stressed rigid Q^4-Q^4 and isostatically rigid Q^4-Q^3 pairs.

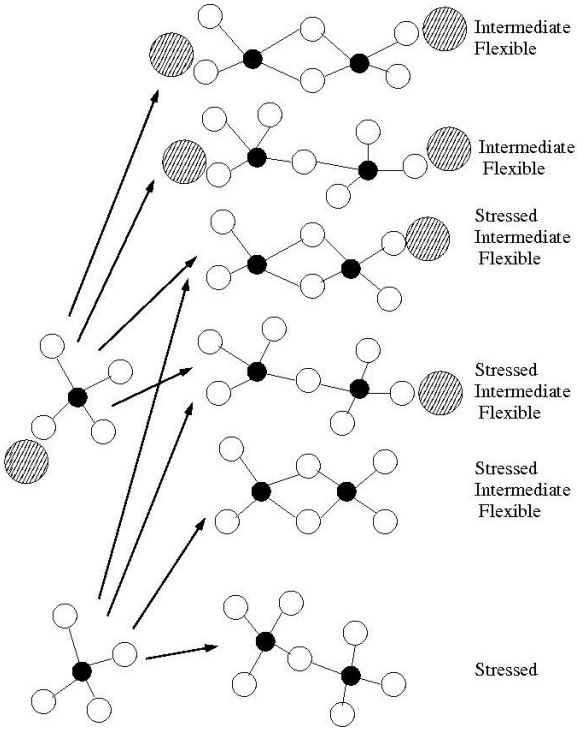

Fig. 2. Q^4, Q^3 cluster construction in a typical SiX_2-M_2X glassy system leading to various corner- (CS) and edge-sharing (ES) Q^j-Q^j pairs which exist only in the elastic phases listed on the right and contribute to the free carrier density.

Floppy modes start to proliferate in the flexible phase at $x>x_r$ when $f^{(2)}$ (equation (2)) becomes non-zero. This allows an easier local deformation of the network thus increasing the hopping rates and should reduce the energy required to create doorways between two vacant sites. We write

therefore the strain energy as: $E_m^{flex}=E_m^{stress}-\square f^{(2)}$ where $\square$ is a typical floppy mode energy given by experiment [35]. In the flexible phase, E_m is reduced by a quantity $\square f^{(2)}$ when compared to the stressed rigid phase. One is then able to write a conductivity of the form:

$$\sigma = n_L^{(2)} \mu^{(2)} = n_L^{(2)} e^{-\beta E_m} \tag{6}$$

2.2 Results

Results of the rigidity model for σ are displayed in Fig. 3 for various parameters E_c. They show that the underlying mechanical nature of the host networks strongly affects the ion transport. In the stressed rigid phase, the stress energy is high and the number of hopping possibilities is low (only between CS and ES Q^4-Q^3 pairs), combined with a low free carrier density. The conductivity is therefore found to be low and to depend only weakly on the modifier concentration. The order of magnitude of $\square$ is determined by the value of E_c, i.e. the interaction energy between the cation and its anionic site.

In the intermediate phase, new cation pairs (and thus hopping possibilities, Fig. 2) appear and lead to a mild increase of $\square$. The first order stress transition at x_r that usually separates the stressed rigid phase and the IP [17, 19, 20, 36] is seen as a break in the slope of σ vs x. The jump seen at the rigidity transition composition $x=x_s$ depends on the parameter E_c (or inverse temperature at fixed E_c, because of the Boltzmann factor, see equ. (2)), whereas the location of the stress transition itself (and the corresponding width of the IP) will only depend on the structure *via* an allowed ES fraction [19, 20]. Large values for the Coulombic energy E_c will lead to large jumps in conductivity at the stress transition. One expects therefore to observe the first order stress transition rather in electrolytes involving heavy cations (such as Ag or K) than in electrolytes using more lighter ones (Li). Similarly, one expects to see the jump increase with decreasing temperature.

Conductivity displays a second threshold at the rigidity transition $x=x_r$ when floppy modes start to proliferate and decrease the migration energy barrier. It clearly suggests that flexibility promotes conductivity. The latter can indeed increase when available degrees of freedom appear that facilitate local deformations of the network and the creation of pathways for conduction. The present results furthermore suggest that the increase of the number of possible hopping processes (in the IP) contribute only weakly to the dramatic increase of $\square$ that mostly arises from the fact that in the flexible phase $f^{(2)} \neq 0$.

3. Experimental

How do experimental results compare with the theory of ionic conduction based on flexibility/rigidity of networks? Fairly well, as we will illustrate next for systems where complete data on conductivity as a function of glass composition is available such as the alkali-silicates and -germanates, and silver phosphates. In each case we find evidence for intermediate phases with conductivity increasing precipitously once networks become flexible as predicted by the theory.

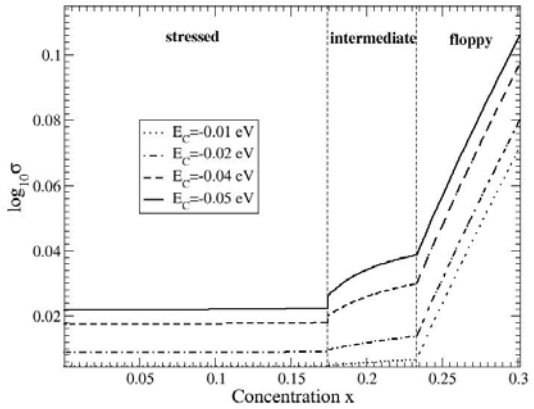

Fig. 3. Conductivity in a (1-x)SiX_2-xM_2X glassy system as a function of the modifier concentration for various Coulombic energies E_c. Here E_m^{stress}=0 and Δ=0.05eV. The location of the thresholds x_s and x_r and the width of the IP are fixed by an ES tetrahedral fraction of 34%.

3.1 Sample synthesis

Glass samples were synthesized by reacting precursors in a dry ambient environment. Melts were then poured in special troughs resulting in platelets of about 10 mm diameter and 2 mm thickness. Platelets were thermally relaxed by cycling through T_g. Samples were polished, and the Pt electrodes deposited. Electrical conductivity of glasses is measured by a two-electrode impedance spectroscopy setup. Samples are hold by a weak spring between two platinum electrodes, which measure current passing through a sample while a known voltage is applied. The whole apparatus is placed in a horizontal tubular furnace, the temperature of which is raised to about

T_g + 50°C at a rate of 2°C/min. The sample temperature is measured by a Pt/Pt-Rh(10%) thermocouple placed near the test specimen. Complex impedance Z=Z'+iZ'' of a specimen is measured by a Solartron SI 1260 impedance analyzer controlled by the LabView software. Frequency was varied typically is in 1 MHz < υ < 1 Hz range, and was scanned over 19 points for each measurement. All data are acquired automatically at two-minute intervals. The electrical resistance R_{dc} is read at the high-frequency intersection of the polarisation semi-circle with the *x*-axis in the complex diagram (Cole-Cole plot). The static conductivity, σ_{dc} is obtained from sample resistance R_{dc}, its thickness *t* and surface area *S* covered by platinum.

3.2 Alkali and alkaline earth silicates

We review here data on the systems *(1-x)SiO_2-xM_2O* with *M=Li, Na, K* and *(1-x)SiO_2-xMO* with *M=Ca,Ba*. Although these glasses have moderate conductivities (10^{-4} Ω^{-1}cm^{-1}) at room temperature, they have received considerable attention both experimentally and in simulations because of their applications in domestic glasses and their abundance in magmas [37]. We should stress that alkaline earth silicate glasses have generally higher liquidus temperature as well as glass temperature (T_g) than alkali silicates [38]. We measured electrical conductivity of the two systems xBaO(1-x)SiO_2 and xCaO-(1-x)SiO_2 in their glass-forming range *i.e.* 25<x<37 and 41<x<55 mol% of alkaline earth oxide respectively. The data for alkali silicates are taken from the literature.

The behaviour of σ_{dc} with alkali and alkaline earth composition is represented in figs. 4 and 5. The trend with composition obviously exhibits two distinct conduction regimes; a first one at low modifier concentration where the conductivity is negligibly small, and a second one where σ_{dc} displays an exponential growth or power-law behaviour. For that reason, σ_{dc} is sometimes plotted on a log-scale. From Figs 4 and 5, it becomes clear that

Table 1. Predicted threshold compositions x_c in alkali- and alkaline-earth silicates estimated from global Maxwell counting.

System	Threshold composition x_c	Reference
(1-x)SiO_2-xLi_2O	0.25	[40]
(1-x)SiO_2-xNa_2O	0.20	[19, 20]
(1-x)SiO_2-xK_2O	0.17	[41]
(1-x)SiO_2-xCaO	0.50	[42]
(1-x)SiO_2-xBaO	0.29	[43]

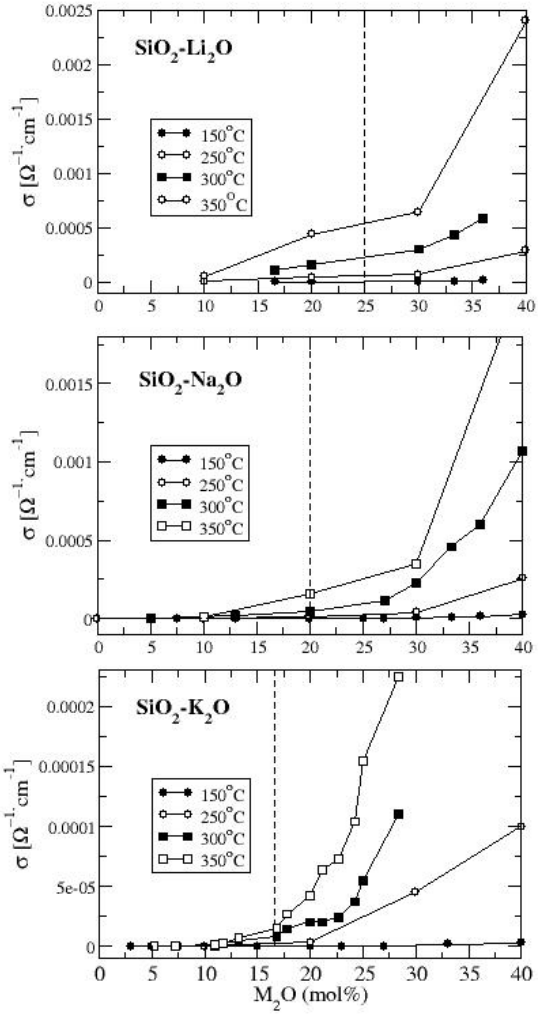

Fig.4. Dc conductivity in glassy alkali silicates as a function of modifier concentration (M=Li, Na and K). The vertical broken lines correspond to the Maxwell rigidity threshold. Lithium and sodium: data from [44, 45]. Potassium: data from [44-48].

the onset of ionic conductivity in the second compositional interval is related with the breakdown of the stressed-rigid network. In calcium silicates, the almost constant value of σ in the low calcium region and sudden increase for x > 0.47 has also been obtained in simulations and experiments for the molten state [39], suggesting that molten and glassy states behave similarly

Enumeration of bond-stretching and bond-bending constraints within the Maxwell approach leads to rigidity thresholds (Table I) that are quite close to the observed thresholds in conductivity, i.e., the composition when a substantial increase sets in.

In alkali-and alkaline-earth-silicate systems, conductivity thresholds are found to shift with the size of the modifier cation, and these shifts correlate well with the anticipated shift of the flexibility/rigidity transition (Table I). This links ionic conductivity to glass network elasticity and structure. In this picture, the major consequence is that carrier concentration does not dominate the conductivity, as widely reported but an increase of network flexibility does.

In fact, the interpretation of the dc conductivity with composition derives from our proposed model described in the previous section. When $x = x_r$, the number of floppy modes vanishes and the network undergoes a rigid-to-flexible transition. For $x < x_r$, the system is stressed rigid, *i.e.* it contains more constraints than degrees of freedom per atom. This means that the mobility of the modifier cation is weak. The latter has to then overcome a strong mechanical-deformation energy to create doorways in order to move from one vacant site to another. This deformation energy vanish in an ideal

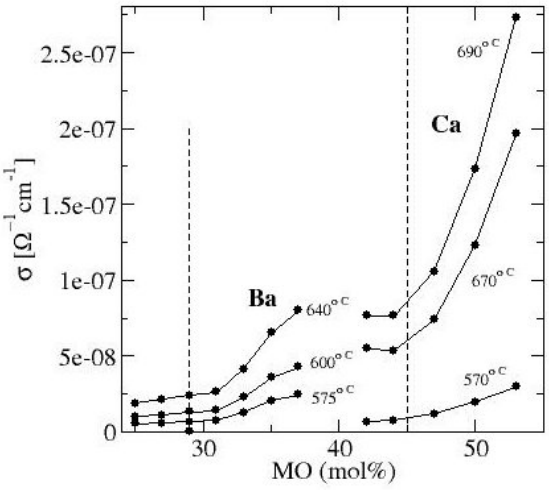

Fig 5. Dc conductivity in glassy alkaline earth silicates (1-x)SiO_2-xMO as a function of modifier concentration (M=Ca or Ba). The vertical broken lines correspond to the Maxwell rigidity threshold. Note that in calcium-silicates the rigidity threshold shifts from x_c=50% to lower concentrations of ~45%.The shift correlates well with vibrational signature of the rigidity transition from Raman scattering [42, 43]. For Ba-silicates, the rigidity transition is predicted near x_c = 29% (Table 1) and is also observed close to that value in conductivity and vibrational spectroscopy (see Fig.7c)

flexible network [23, 24] when only bond-bending and bond-stretching forces are considered at $x>x_c$. The same behaviour is obtained [49] for the. related elastic constants C_{11} and C_{44}. Therefore, percolation of flexibility produces the percolation of the cation mobility resulting in a substantial increase of the mobility thus of the conductivity.

In solid electrolytes such as the present alkali and alkaline earth silicates, it is often believed that it is the carrier concentration that dominates the conductivity [50]. In the strong electrolyte model, the cation electrostatic Coulombic energy barrier has to be overcome to ensure conduction. On the other hand, in the weak electrolyte model a dissociation energy is needed to create the mobile carrier [51]. These two pictures remain of course valid as long as the sizes of the cations are weak compared to the interstices of the glass network.

Connection with the popular conductivity channel picture can also be made [52,53]. This picture has received some support from Molecular Dynamics simulations in the sodium silicates. In these glasses, the rigid to flexible transition occurs (Table I) at the alkali concentration $x_r = 0.20$, a concentration that is very close to the reported threshold concentration separating intrachannel cation hopping from network hopping [54]. The latter needs a strong mechanical deformation which is only possible in a flexible network, whereas the latter involves only a weak mechanical deformation of the network, since the motion occurs only in macroscopic holes of the network.

Signature for the onset of ionic conduction induced by flexibility receives also support from the study of the conductivity in molten calcium silicates. In the liquid phase, an increase in conductivity for $x>x_c$ is still observed but with values that are substantially higher compared to the glass. In this case, □ can be fitted with a Vogel-Fulcher-Tamman (VFT) law: of the form:

$$\sigma T = A\exp\left[\frac{-\Delta}{(T-T_0)}\right] \tag{7}$$

It appears that the pseudo-activation energy Δ is constant for the two values in the flexible region (Δ = *2733.0* and *2740.7 K* for, respectively, $x = 0.44$ and $x = 0.5$), while it increases for the composition $x = 0.53$ (Δ = 3008 K). Also, the VFT temperature T_0 at which the diffusion constant (and the underlying relaxation time towards thermal equilibrium) diverges, is very

close to the T_g of the corresponding glass, suggesting that the glass transition is optimal.

Unfortunately, because of the high value of the glass transition temperature in theses alkali and alkaline earth silicates, the calorimetric probe (temperature modulated differential scanning calorimetry (MDSC)) of the intermediate phase and the stress and rigidity transitions cannot be used at present. An alternative signature is given from vibrational thresholds obtained in Raman measurements. For the *(1-x)SiO_2-xCaO* system, the frequency ν and the linewidth Γ of the stressed rigid $SiO_{4/2}$ (Q^4 unit) can be tracked with the calcium composition [42, 55]. The corresponding line (A_1 stretching mode) exhibits a change of regime (Fig. 6) for the line frequency at the concentration $x = 0.50$, consistently with chalcogen analogs [56, 57]. On the other hand, the evolution of the linewidth Γ with x permits to follow the local environment of the Q^4-unit. For $x < 0.50$, Γ remains constant, related to the absence of change in the coupling of this unit with the rest of the network. It is the coupling which makes possible the presence of rigid regions (through isostatic Q^4-Q^3 and stressed Q^4-Q^4 bondings), although the number of flexible Q^2- and Q^1-units is steadily increasing. Above the critical concentration $x=0.50$, the sharp drop of Γ clearly shows decoupling of the Q^4-unit with respect to the network (Fig. 7), signifying decoupling of stressed rigid regions and thus percolation of flexibility. Similarly, one sees that at the composition where the barium conductivity sets in (x=29%, see Fig. 5), a pronounced drop in the stressed rigid Q^4 population (or corresponding Raman intensity) can be observed (Fig. 6). These results clearly suggest that the stressed-rigid to flexible transition detected from vibrational spectroscopy correlates well with the conductivity threshold. Can intermediate phases be detected as well? Yes, as we will show next in calorimetric experiments using MDSC, which precisely probe boundaries of the IP.

3.3 Alkali germanates

Alkali germanates *(1-x)GeO_2-xM_2O* (*M=Li,Na,K*) are prototypical oxides, with physical properties varying anomalously with alkali oxide content. The molar volume of glasses show indeed a broad global minimum near e.g. 18% of sodium, which has been termed as the germanate anomaly [59]. Its origin is still actively debated [60-62].

We have investigated Sodium Germanate glasses (M=Na) and some of the results appear in Fig.7. The observation of a reversibility window fixes the three elastic phases. We observe in fact (right axis) a deep reversibility window (RW) with abrupt edges in ΔH_{nr} (x) for 14% < x <

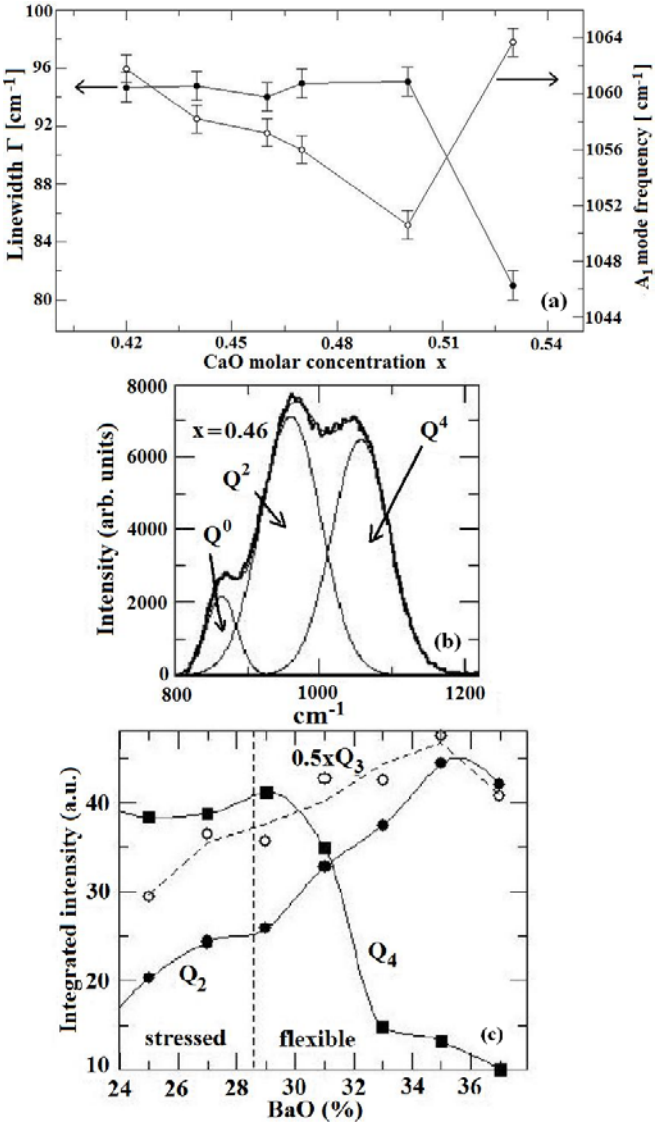

Fig. 6 (a). A_1 mode frequency ν (open circles) and linewidth Γ (filled circles) of the Q^4 line as a function of Ca concentration x in (1-x)SiO_2-xCaO glasses, (b) shows a part of the Raman lineshape where modes of relevant Q-species are identified at x = 0.46; 850 cm^{-1} (Q^0-unit) and 950 cm^{-1} (Q^2-unit) from [58], and (c) Integrated intensity of Raman Q^n modes in (1-x)SiO_2-xBaO glasses. The vertical broken line corresponds to the rigidity transition estimated from Maxwell counting (Table I).Note that at x > 29%, Q^2, Q^3 species increase at the expense of Q^4 species as networks become flexible.

< 19%. The conductivity measurements on sodium germanate glasses have also been reported by several groups [63] and do indeed reveal a precipitous increase once x > 20%, as will be discussed elsewhere.

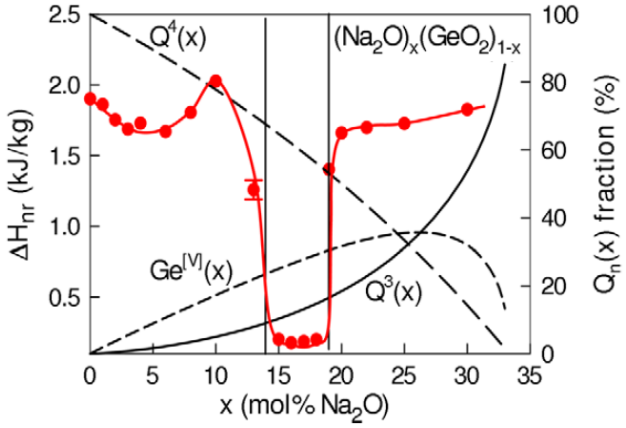

Fig 7. Compositional trends in ΔH_{nr} of $(Na_2O)_x(GeO_2)_{1-x}$ from m-DSC [61].Model calculations reveal Q^3 species to increase at the expense of Q^4 species once x > 20%. See details in ref [61].

3.4 Silver phosphates

Electrical conductivity of silver phosphates $(AgI)_x(AgPO3)_{1-x}$ has been measured by several authors although a consensus on the data has been elusive. In one study [64] a percolative transition is reported near *x = 0.3*, while in another one conductivity is found to increase [65] more or less in steps. We showed that the variability of the data is likely due to water contamination. Our work was on specifically prepared dry samples [66, 67]. Our glass transition temperatures $T_g(x)$ are at least *50°* to *100°C* higher than those reported hitherto [64, 65, 68] and their physical properties display thresholds near *x = 0.095* and *x = 0.379*. These findings show that traces of water in these glasses alter their physical behaviour profoundly and that properties of flexibility and rigidity of backbones commonplace in covalent systems [69-71], is a concept that extends to solid electrolyte glasses as well, and that fast ion-conduction is promoted qualitatively when glasses become flexible.

In order to examine glass transitions and in particular to determine the reversibility window, Modulated-Differential Scanning Calorimetry (MDSC) experiments were performed on these glasses from TA Instrumments at a heating rate of 3°C/min and modulation rate of 1°C/min. The observed variations in $T_g(x)$ and the non-reversing enthalpy, $\Delta H_{nr}(x)$, of present dry $xAgI\text{-}(1\text{-}x)AgPO_3$ glasses are summarized in Figs. 8(a) and 8(b). Here *x* represents the mole fraction of *AgI*. We find $T_g(x)$ to monotonically decrease as *AgI* content increases, but the $\Delta H_{nr}(x)$ term to vary

nonmonotonically displaying a rather striking global minimum (the reversibility window [70]) in the 9.5%< x<37.8% range. At higher *x (>45%)*, the $\Delta H_{nr}(x)$ term decreases again as glasses depolymerize. Variations in room temperature electrical conductivity, $\sigma(x)$, appear in Fig. 8(c), and show increases in steps, one near *9.5%* and another near *37.8%*. For comparison, we have shown in Figs. 8(a) and 8(c) variations in $T_g(x)$ and in $\sigma(x)$ reported earlier [65]. The present findings on dry samples differ significantly from previous ones in the field.

Room temperature conductivities of our dry glasses increase with x and display a change in regime near $x_{c1} = 0.095$ and near $x_{c2} = 0.378$. The increase of conductivity observed at $x > x_{c2}$ can be described by a power-law variation:

$$\sigma (x) = B (x – x_c(2))^{\mu} \qquad (8)$$

with a value of $\mu = 1.78$ and of $x_c(2) = 0.378$ as shown in Fig. 8c.

The thermal, and electrical results presented above lead to the following interpretation. The reversibility window, $0.095 < x < 0.378$, in analogy to the case of covalent glasses [69, 71], we identify with the *Intermediate phase* of the present solid electrolyte glasses. The base $AgPO_3$ glass is weakly *stressed-rigid*, and AgI alloying steadily lowers the connectivity of the chain network as reflected in the reduction of $T_g(x)$ and the emergence of the first sharp diffraction peak [72] near $0.7\ A^{-1}$ in neutron scattering experiments.

From an electrical point of view, addition of the electrolyte salt *AgI* to the insulating base $AgPO_3$ glass serves to provide Ag^+ carriers, and to also elastically soften the base glass. At low *x* (< *0.095*), Ag^+ ions undergo *localized* displacements in backbones as suggested by Reverse Monte simulations [72], a view that is independently corroborated by intrinsically *stressed-rigid* character of these glasses in the present work. With increasing *AgI*, and particularly in the Intermediate Phase, backbones become stress-free [71] and Ag^+ displacements increase as do conductivities (Fig.8c). At higher x (> *0.378*), backbones become elastically flexible and electrical conductivities increase precipitously as carriers freely diffuse [72] along percolative pathways. Thus, although carrier concentrations increase monotonically with *x*, the observed thresholds in $\sigma(x)$ suggest that it is network rigidity (flexibility) that controls fast-ion conduction by suppressing (promoting) Ag^+ ion migration. The kinks in room temperature conductivities (Fig.8c) near the two elastic phase boundaries (x_{c1}, x_{c2}), most likely, seem to be generic features of electrolyte glasses as they have been found in other glassy electrolytes as well such as the potassium germanate system.

Inspection of the behavior of the conductivity with iodine composition shows also that $\sigma(x)$ follows exactly the predicted behavior from the rigidity ionic model described previously, i.e. one has a constant

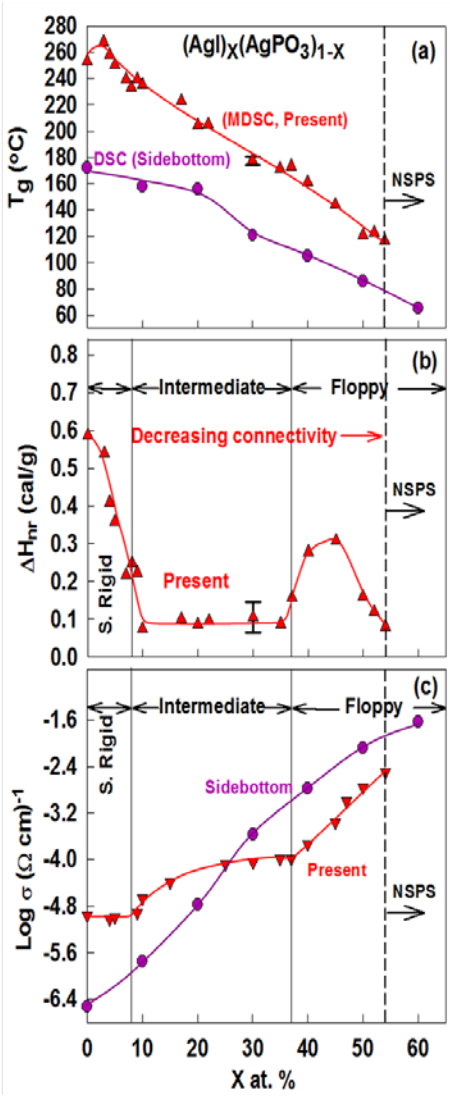

Fig 8. Variations in (a) $T_g(x)$, (b) non-reversing enthalpy, (c) room temperature conductivities, $\sigma(x)$ in dry$(AgI)_x(AgPO3)_{1-x}$ glasses synthesized in the present work (black triangles) and those reported by Sidebottom (purple circles) [65]. At x > 55 %, Tg's decrease to 65°C, a value characteristic of AgI glass (see Ref. [73]).

and low value for the conductivity [illegible] in the stressed rigid phase with a marked jump at the stress transition located at x_{c1}=9.5%. In the intermediate phase, [illegible] with x in the semi-log plot, similarly to what is obtained in Fig. 3. Finally, a power-law behavior is obtained in the flexible phase. One should also remark that if the

temperature is changed (data of Fig. 8 have been recorded at room temperature), the jump seen at x_{c1} decreases as anticipated from the ionic-rigidity model (Fig. 3) and observed from experiments performed at three different temperatures (Fig. 9). Obviously, the jump of the first order stress transition is temperature dependent and decreases with increasing temperature.

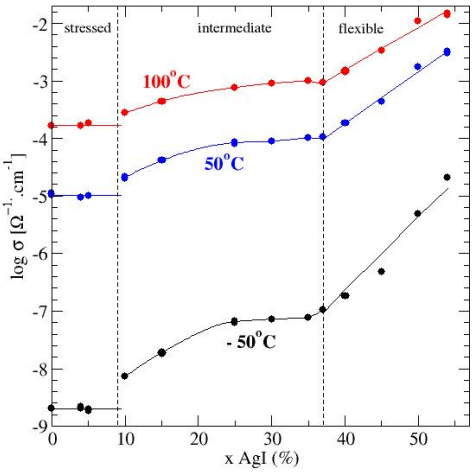

Fig 9. Variations in conductivities $\sigma(x)$ in dry $(AgI)_x(AgPO3)_{1-x}$ glasses for different temperatures. Note the jump of σ at the stress transition.

4. Network Flexibility and Non-Arrhenius T-variation of Conductivity

Rigidity effects manifest in another well-known phenomenon observed in solid electrolytes, the non-Arrhenius behaviour with temperature [74-77]. In fact, there are limitations in the dc conductivity of several groups of glasses, especially superionic conducting glasses which display conductivities up to 10^{-1} $\square^{-1}$.cm^{-1} at room temperature. These limitations appear when the temperature is increased and saturation effects onset that lead to the departure of Arrhenius behaviour in conductivity.

4.1 Potassium silicates

We have focused on one particular system which is the potassium silicate glass of the form $(1-x)SiO_2$-xK_2O. Details of the synthesis can be found in Ref. [41] and the description of the experimental setup for conductivity measurements have been given above. We have focused on

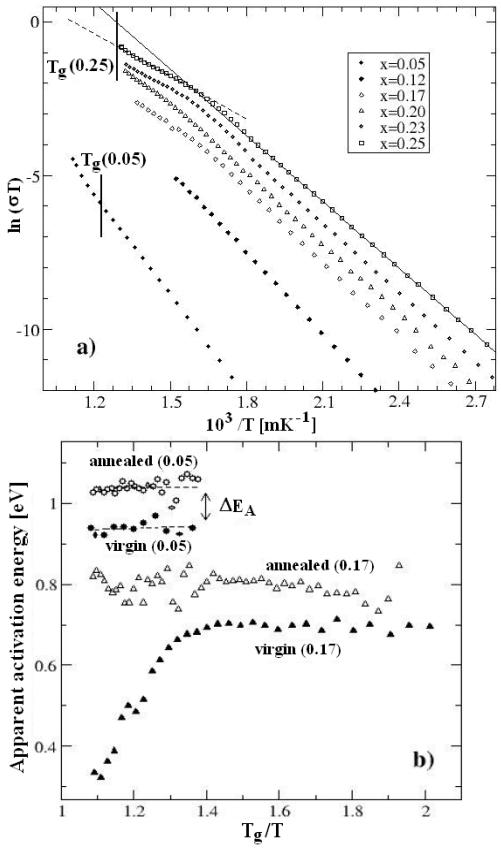

Fig 10: a) Arrhenius plots of conductivity in $(K_2O)_x(SiO_2)_{1-x}$ glasses in their virgin state, as a function of potassium oxide concentration x. The solid line corresponds to a low-temperature Arrhenius fit for the x=0.25 composition. The vertical lines indicate T_g at two compositions (0.05 and 0.25). b) Effect of sample annealing on conductivity of glass compositions at x = 0.05 and 0.17. Conductivity of virgin glasses: x=0.05 (●) and x=0.17 (▲) compared to that of the corresponding annealed glasses (○, Δ).

the temperature study of the conductivity for various potassium concentrations in the virgin (i.e. as-quenched) and annealed state (Fig. 10a**)** shows the Arrhenius plots of the ionic conductivity for the different virgin potassium silicates. One can first observe that glasses at low potassium concentration (e.g., *x =0.05*) display an almost perfect Arrhenius behavior with respect to the temperature while those at high concentration exhibit a clear saturation manifested by a significant curvature at high temperatures that signals departure from Arrhenius behavior.

Fig. 10b highlights the fact that annealing removes the curvature and brings the conductivity in the glass to Arrhenius behavior even though the absolute value of conductivity decreases with respect to the virgin state. Such a This is a feature that has been observed by Ingram and co-workers [78] for oxysalt chalcogenides involving iodine anions and identified with the dynamic temperature dependent restructuring iodine sublattice. Densification was claimed to play the key role and it appears that this seems also the case in the present system as density changes with annealing are relatively small for compositions lying in the stressed rigid phase in the silica-rich compositional region.

Fig. 11 shows for two virgin and two annealed potassium glasses (*x=0.05* and *0.17*) the apparent activation energy that is computed as the running slope between adjacent temperature conductivity data points. We note from the figure that in the case of the latter virgin glass, the difference in activation energy between the low and the high temperature side is about 0.4 eV (0.7 eV at *T*=400 K and 0.3 eVat *T*=700 K). For comparison, the corresponding reported difference for the highest saturated silver superconducting chalcogenide was about 0.15 eV. Therefore, the effect of saturation does not appear to be restricted to chalcogenides [74]. On the other hand, both virgin and annealed (*x*=0.05) glasses display a more or less constant activation energy (respectively found as 1.04 and 0.93 eV). From the observations made on both figures, it becomes clear that a dramatic change in regime occurs in the composition interval *0.12< x<0.17*. This change is also observable from the low-temperature activation energy difference between the annealed and virgin state $\Delta E_A = E_A(annealed) - E_A(virgin)$ which displays a significant drop in the aforementioned compositional interval (Fig. 11). From this figure, one clearly observes that a critical alkali concentration x_c =0.14 separates glasses with Arrhenius behaviour (AB) from those displaying non-AB. The annealing of the glasses leading to densification tends to reduce the saturation which suggests that densification with annealing may be responsible for the loss of non-Arrhenius variation. With the observation of an intermediate phase in the compositional interval [0.145-10.65], an analysis from bond constraint theory can be performed to locate the mean-field rigidity transition. In silicates, such a transition occurs at the alkali concentration of *x=0.20* when the cation size is small [19, 20]. Due to the potassium cation size (cation radius R_K=1:33 A and R_{Na}= 0.95 A [79]), one expects that a supplementary oxygen angular constraint is broken because the bridging bond angle Si-O-Si in the glass network is found to display wide excursions (135-155^o) around a mean angle that is much larger [32] than in the sodium analog [80]. According to this enumeration, a rigid to floppy transition is predicted [41] at the concentration of x_c=0.14, close to the observed threshold observed in Fig. 11(a). The study of the local structure of potassium silicate glasses

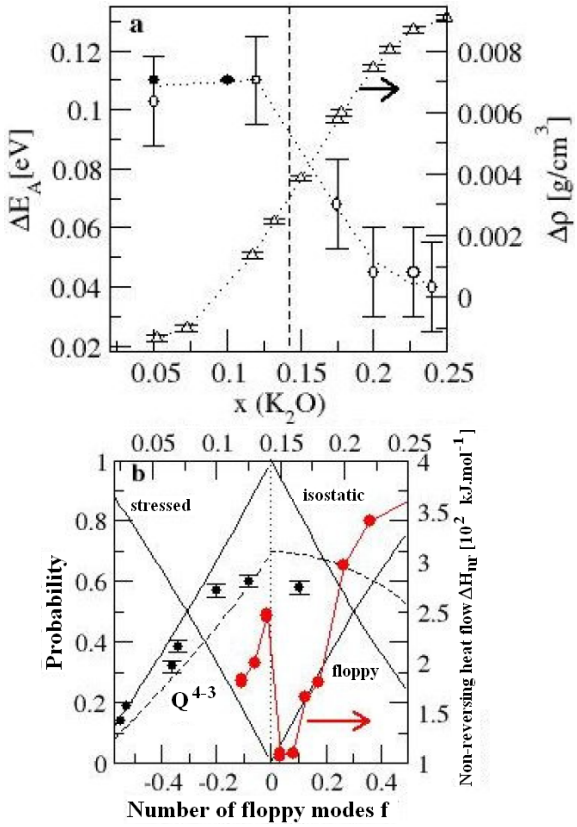

Fig. 11. (a) Low-temperature activation energy difference ΔE_A (open circles) between the virgin and annealed samples [41], together with previous results obtained (filled circles [81]), as a function of potassium concentration x.. (b) Relative fraction of Q^4-Q^3 pairs (filled circles, from [82]) together with theoretical prediction of the probability of Q^4-Q^3 pairs(broken line) computed from SICA [19, 20]*. The solid lines represent the probability of finding stressed rigid, isostatically rigid, and floppy clusters. The lower horizontal axis is scaled in atomic number of floppy modes f. The vertical dotted line corresponds to the mean-field rigidity transition $x_c = 0.14$ where $f = 0$. The right axis shows the corresponding intermediate phase from heat flow measurements [47, 48]*

obtained from NMR investigation provides a supplementary evidence [79] about the location of the rigid to floppy transition because constraint counting can be applied onto the observed Q^n speciation to yield the probability of finding stressed rigid and floppy structures in the network

(Fig. 11(b)). Furthermore, we notice that a cluster composed of a Q^4 and Q^3 tetrahedron (a ''$K_2Si_4O_9$-like'' cluster) is optimallyconstrained (isostatically rigid, satisfying n_c=3). The corresponding probability of finding the latter is found to be maximum around the same critical concentration of x_c=0.14. Thus at this composition the network is mainly stress-free. For larger concentrations, size increasing cluster approximations (SICA) predict the growing emergence of floppy clusters such as Q^3-Q^3 pairs should appear.

5. Conclusions

Compositional variation of ionic conductivity, σ(x), in alkali-, and alkaline-earth silicates and germanates, and the solid electrolyte glass (AgI)x(AgPO3)1-x provide evidence of three regimes of behaviour with two distinct thresholds (x_{c1},x_{c2})). At low electrolyte additive concentration, $x < x_{c1}$, conductivities are minuscule because the system is stressed-rigid, *i.e.* it contains more constraints than degrees of freedom per atom, and mobility of cations is very small. Cations have to overcome strong mechanical-deformation energy to create doorways to hop from one anionic site to another. In the second regime, $x_{c1} < x < x_{c2}$, conductivities increase as networks become stress-free and mobilities increase as elastic deformation energy decrease. In the third regime at high electrolyte additive concentrations, $x > x_{c2}$, conductivities increase as a power-law. In this regime, the deformation energy vanishes in an ideal flexible network when only bond-bending and bond stretching forces are considered. These thresholds identified from calorimetric and vibrational behavior of these glasses are found to correlate well with those observed in ionic conductivities. A model of ionic conductivity based on flexibility and rigidity of solid electrolyte glassy networks is developed and it provides a good theoretical description of these observations. These results demonstrate that ionic conductivities are closely correlated to network elastic behavior or network connectivity or network structure.

Acknowledgements

It is a pleasure to acknowledge discussions with Professor Malcolm Ingram, and Ping Chen during the course of this work. The calorimetric measurements on Potassium silicate glasses were performed by Dr. Tao Qu. This work is supported by NSF grant DMR 04-56472.

References

[1] M. D. Ingram, Phil. Mag. B **60**, 729 (1989).
[2] C. A. Angell, Annu. Rev. Phys. Chem. **43**, 693 (1992).
[3] D. Ravaine, J. Non-Cryst. Solids **38-9**, 353 (1980).
[4] Y. Vaills, T. Qu, M. Micoulaut, F. Chaimbault, P. Boolchand, J. Phys. Condens. Matter **17**, 4889 (2005).
[5] G. N. Greaves, K. L. Ngai, J. Non-Cryst. Solids **172**, 1378 (1994).
[6] M. D. Ingram, Phys. Chem. Glasses **28**, 215 (1987).
[7] F. S. Howell, R. A. Bose, P. B. Macedo, C. T. Moynihan, J. Phys. Chem. **78**, 639 (1974).
[8] C. A. Angell, Solid State Ionics **18-9**, 72 (1986).
[9] L. M. Torell, C. A. Angell, British Polymer Journal **20**, 173 (1988).
[10] M. D. Ingram, C. T. Imrie, J. Ledru, J. M. Hutchinson, J. Phys. Chem. B **112**, 859 (2008).
[11] D. Selvanathan, W. J. Bresser, P. Boolchand, B. Goodman, Solid State Commun. **111**, 619 (1999).
[12] P. Boolchand, G. Lucovsky, J. C. Phillips, M. F. Thorpe, Phil. Mag. **85**, 3823 (2005).
[13] D. Selvanathan, W. J. Bresser, P. Boolchand, Phys. Rev. B **61**, 15061 (2000).
[14] D. G. Georgiev, P. Boolchand, M. Micoulaut, Phys. Rev. B **62**, R9228 (2000).
[15] P. Boolchand, D. G. Georgiev, B. Goodman, J. Optoelectron. Adv. Mater. **3**, 703 (2001).
[16] P. Boolchand, X. Feng, W. J. Bresser, J. Non-Cryst. Solids **293**, 348 (2001).
[17] M. F. Thorpe, D. J. Jacobs, M. V. Chubynsky, J. C. Phillips, J. Non-Cryst. Solids **266**, 859 (2000).
[18] M. V. Chubynsky, M. A. Briere, N. Mousseau, Phys. Rev. E **74**, 016116 (2006).
[19] M. Micoulaut, J. C. Phillips, Phys. Rev. B **67**, 104204 (2003).
[20] M. Micoulaut, Phys. Rev. B **74**, 184208 (2006).
[21] J. Barre, A. R. Bishop, T. Lookman, A. Saxena, Phys. Rev. Lett. **94**, 208701 (2005).
[22] J. C. Phillips, J. Non-Cryst. Solids **34**, 153 (1979).
[23] M. F. Thorpe, J. Non-Cryst. Solids **57**, 355 (1983).
[24] H. He, M. F. Thorpe, Phys. Rev. Lett. **54**, 2107 (1985).
[25] M. Zhang, P. Boolchand, Science **266**, 1355 (1994).
[26] H. Maekawa, T. Maekawa, K. Kawamura, T. Yokokawa, J. Non-Cryst. Solids **127**, 53 (1991).
[27] A. Pradel, G. Taillades, M. Ribes, H. Eckert, J. Non-Cryst. Solids **188**, 75 (1995).
[28] O. L. Anderson, D. A. Stuart, J. Am. Ceram. Soc. **37**, 573 (1954).
[29] S. R. Elliott, A. P. Owens, Phys. Rev. B **44**, 47 (1991).
[30] L. F. Perondi, R. J. Elliott, R. A. Barrio, K. Kaski, Phys. Rev. B **50**, 9868 (1994).
[31] R. J. Elliott, L. Perondi, R. A. Barrio, J. Non-Cryst. Solids **168**, 167 (1994).

[32] I. Farnan, P. J. Grandinetti, J. H. Baltisberger, J. F. Stebbins, U. Werner, M. A. Eastman, A. Pines, Nature **358**, 31 (1992).
[33] S. R. Elliott, A. P. Owens, Phil. Mag. B **60**, 777 (1989).
[34] S. R. Elliott, Solid State Ionics **27**, 131 (1988).
[35] H. Uhlig, S. Bennington, J. B. Suck, J. Phys. Condens. Matter **12**, 6979 (2000).
[36] M. A. Brière, M. V. Chubynsky, N. Mousseau, Phys. Rev. E **75**, 56108 (2007).
[37] B. Mysen, P. Richet, Silicate glasses and melts: properties and structure (Elsevier, Amsterdam; Boston, 2005).
[38] O. V. Mazurin, M. V. Streltsina, T. P. Shvaiko-Shvaikovskaya, Hanbook of Glass Data Part A (Elsevier, 1983).
[39] D. K. Belashnko, Inorg. Mater. **32**, 160 (1996).
[40] M. Micoulaut, Am. Mineral **93** (2008, in press).
[41] M. Malki, M. Micoulaut, F. Chaimbault, Y. Vaills, Phys. Rev. Lett. **96**, 145504 (2006).
[42] M. Malki, M. Micoulaut, F. Chaimbault, Y. Vaills, P. Simon, Europhys. Lett. **64**, 661 (2003).
[43] C. Bourgel, M. Micoulaut, M. Malki, P. Simon, Physical Review B (submitted) (2008).
[44] K. Otto, M. E. Milberg, J. Am. Ceram. Soc. **51**, 326 (1968).
[45] O. V. Mazurin, E. S. Borisovskii, Zh. Tekh. Fiz. **27**, 275 (1957).
[46] K. K. Evstrop'ev, V. K. Pavlovskii, Inorg. Mater. **3**, 673 (1967).
[47] F. Chaimbault, Ph.D. Thesis, Université d'Orléans (2004).
[48] F. Chaimbault, Y. Vaills, M. Micoulaut, P. Boolchand, (unpublished results).
[49] D. S. Franzblau, J. Tersoff, Phys. Rev. Lett. **68**, 2172 (1992).
[50] S. W. Martin, C. A. Angell, J. Non-Cryst. Solids **83**, 185 (1986).
[51] D. Ravaine, J. L. Souquet, Phys. Chem. Glasses **18**, 27 (1977).
[52] E. Sunyer, P. Jund, R. Jullien, Phys. Rev. B **65**, 214203 (2002).
[53] P. Jund, W. Kob, R. Jullien, Phys. Rev. B **64**, 134303 (2001).
[54] G. N. Greaves, K. L. Ngai, Phys. Rev. B **52**, 6358 (1995).
[55] M. Micoulaut, M. Malki, P. Simon, A. Canizares, Phil. Mag. **85**, 3357 (2005).
[56] B. Norban, D. Pershing, R. N. Enzweiler, P. Boolchand, J. E. Griffiths, J. C. Phillips, Phys. Rev. B **36**, 8109 (1987).
[57] X. W. Feng, W. J. Bresser, P. Boolchand, Phys. Rev. Lett. **78**, 4422 (1997).
[58] P. McMillan, B. Piriou, Bulletin De Mineralogie **106**, 57 (1983).
[59] A. O. Ivanov, K. S. Estropiev, Dokl. Akad. Nauk. SSSR **145**, 797 (1962).
[60] G. S. Henderson, J. Non-Cryst. Solids **353**, 1695 (2007).
[61] K. Rompicharla, D. I. Novita, P. Chen, P. Boolchand, M. Micoulaut, W. Huff, J. Phys.: Condens. Matter **20**, 202101 (2008).
[62] G. S. Henderson, M. E. Fleet, J. Non-Cryst. Solids **134**, 259 (1991).
[63] J. F. Cordaro, M. Tomozawa, Phys. Chem. Glasses **25**, 27 (1984).

[64] M. Mangion, G. P. Johari, Phys. Rev. B **36**, 8845 (1987).
[65] D. L. Sidebottom, Phys. Rev. B **61**, 14507 (2000).
[66] D. I. Novita, P. Boolchand, Phys. Rev. B **76**, 184205 (2007).
[67] D. I. Novita, P. Boolchand, M. Malki, M. Micoulaut, Phys. Rev. Lett. **98**, 195501 (2007).
[68] C. Tomasi, P. Mustarelli, A. Magistris, M. P. I. Garcia, J. of Non-Cryst. Solids **293**, 785 (2001).
[69] T. Qu, D. G. Georgiev, P. Boolchand, M. Micoulaut, in Supercooled Liquids, Glass Transition and Bulk Metallic Glasses, edited by T. Egami, A. L. Greer, A. Inoue and S. Ranganathan (Materials Research Society, Warrendale, PA, 2003), Vol. 754, p. 157.
[70] S. Chakravarty, D. G. Georgiev, P. Boolchand, M. Micoulaut, J. Phys. Condens. Matter **17**, L1 (2005).
[71] F. Wang, S. Mamedov, P. Boolchand, B. Goodman, M. Chandrasekhar, Phys. Rev. B **71**, 174201 (2005).
[72] J. D. Wicks, L. Börjesson, G. Bushnell-Wye, W. S. Howells, R. L. McGreevy, Phys. Rev. Lett. **74**, 726 (1995).
[73] P. Boolchand, W. J. Bresser, Nature **410**, 1070 (2001).
[74] J. Kincs, S. W. Martin, Phys. Rev. Lett. **76**, 70 (1996).
[75] S. W. Martin, D. M. Martin, J. Schrooten, B. M. Meyer, J. Phys. Condens. Matter **15**, S1643 (2003).
[76] P. Maass, M. Meyer, A. Bunde, W. Dieterich, Phys. Rev. Lett. **77**, 1528 (1996).
[77] K. L. Ngai, A. K. Rizos, Phys. Rev. Lett. **76**, 1296 (1996).
[78] M. D. Ingram, C. A. Vincent, A. R. Wandless, J. Non-Cryst. Solids **53**, 73 (1982).
[79] Y. Q. Jia, J. Solid State Chem. **95**, 184 (1991).
[80] I. Yasui, Y. Akasaka, H. Inoue, J. Non-Cryst. Solids **177**, 91 (1994).
[81] P. W. Angel, R. E. Hann, A. R. Cooper, J. Non-Cryst. Solids **183**, 277 (1995).
[82] S. Sen, R. E. Youngman, J. Non-Cryst. Solids **331**, 100 (2003).